Visualizing AVAZ Parameter Estimates and Uncertainty

Jon Downton*
CGGVeritas, Calgary, AB, Canada
Jon.Downton@CGGVeritas.com

and

Dave Gray and Torre Zuk
CGGVeritas, Calgary, AB, Canada

Summary

We present a technique to estimate and visualize uncertainty due to random noise for azimuthal AVO attributes in HTI media. With this technique, uncertainty can be efficiently calculated as a by-product of the AVAZ inversion. The visualization technique allows the interpreter to view simultaneously the anisotropic gradient, HTI orientation, and uncertainty.

The uncertainty is proportional to the noise level, is dependent on the geology and is influenced by the acquisition geometry. Because of the nonlinearity of the inversion problem, azimuthal AVO inversion will always produce a positive estimate of the anisotropy gradient even if the media is isotropic; thus it is important that this attribute be examined along with its uncertainty. The interpreter must be confident that any potential anomaly is much larger than its uncertainty. Using this approach, legitimate anomalies due to geology may be distinguished from those due to noise and/or insufficient data.

The uncertainty is calculated following a Bayesian methodology. Although an approximation is required, the method is quite accurate for most situations of interest to the explorationist. By making this approximation, it is possible to calculate the uncertainty as part of the AVAZ inversion, making the whole analysis quite efficient.

Introduction

Azimuthal AVO (AVAZ) has proved to be an important tool for characterizing fracture distributions and directions for hydrocarbon reservoirs (e.g. Al-Marzoug et al., 2004; Gray & Todorovic-Marinic, 2004). However, the AVAZ inversion problem is ill-conditioned and sometimes ill-posed, raising questions about the reliability of the estimates. To help understand and quantify this, Downton and Gray (2006) developed an approximate method to estimate the uncertainty of the AVAZ inversion estimates due to uniform independent Gaussian noise. This paper demonstrates the use of these attributes on a 3D seismic survey from western Canada. In particular, visualization tools are demonstrated which allow the interpreter to simultaneously view the parameters of interest and their uncertainty. This allows the explorationist to distinguish legitimate anomalies due to the geology versus those arising from the noise and inadequate data acquisition.

Method

For the case of an isotropic half-space over an HTI anisotropic half-space, Ruger (2002) shows that the amplitude R versus azimuth Φ for narrow angles of incidence θ is

$$R(\theta,\Phi) = A + \left[B_{iso} + B_{ani}\cos^2\left(\Phi - \Phi_{sym}\right)\right]\sin^2\theta, \tag{1}$$

where A is the P-wave impedance reflectivity, B_{iso} the isotropic gradient, B_{ani} the anisotropic gradient and Φ_{sym} is the symmetry axis of the HTI anisotropic media. The anisotropy gradient is related to the crack density. This along with the symmetry axis Φ_{sym} is of primary interest to the explorationist. Equation (1) as written is nonlinear in B_{ani} and Φ_{sym}, and difficult to solve. Xu and Li (2002) linearized equation (1) using the transformations $B = B_{iso} + B_{ani}/2$, $B_{ani}^2 = 4\left(C^2 + D^2\right)$, $\tan 2\phi_{iso} = D/C$, where $\Phi_{iso} = \Phi_{sym} + 90^0$ resulting in

$$R(\theta,\Phi) = A + \left[B - C\cos 2\Phi - D\sin 2\Phi\right]\sin^2\theta. \tag{2}$$

This is essentially a transformation from polar coordinates to Cartesian coordinates.

Equation (2) may be written more compactly in matrix form **d=Gm** where **d** is the observed reflectivity data, $\mathbf{m}=[A,B,C,D]^{\mathrm{T}}$ is the parameter vector and **G** is the linear operator. The unknown parameter vector **m** may be inferred following a Bayesian methodology. This has the advantage that probability distribution functions (PDFs) of each parameter are produced rather than just one estimate. The uncertainty can be characterized by the distribution itself or some parameterization of it. If uniform uncorrelated Gaussian noise and non-informative priors are assumed, the *a posterior* probability distribution (PPDF) is the multivariate Gaussian distribution with mean

$$\mathbf{m} = \left[\mathbf{G}^{\mathrm{T}}\mathbf{G}\right]^{-1}\mathbf{G}^{\mathrm{T}}\mathbf{d}, \tag{3}$$

and covariance

$$\mathbf{C}_m = \sigma_N^2\left[\mathbf{G}^T\mathbf{G}\right]^{-1} = \begin{bmatrix} \sigma_A^2 & \sigma_{AB} & \sigma_{AC} & \sigma_{AD} \\ \sigma_{AB} & \sigma_B^2 & \sigma_{BC} & \sigma_{BD} \\ \sigma_{AC} & \sigma_{BC} & \sigma_C^2 & \sigma_{CD} \\ \sigma_{AD} & \sigma_{BD} & \sigma_{CD} & \sigma_D^2 \end{bmatrix}, \tag{4}$$

where σ_N^2 is the variance of the Gaussian noise. The diagonal terms of the covariance matrix $\mathbf{C}_{\mathrm{m}}$ are the variances (or uncertainty) of each of the parameters while the off-diagonal elements describe the degree of correlation between the errors. The covariance matrix may be calculated as a by-product of solving equation (3) and thus is efficient to calculate. In fact, if the variance of the noise is set to unity then the uncertainty of various acquisition geometries can be studied since only information about the geometry and geology are needed to specify **G**.

The covariance matrix (equation 4) describes the uncertainty of $\mathbf{m}=[A,B,C,D]^{\mathrm{T}}$, however the interpreter is more interested in the uncertainty of B_{ani} and Φ_{iso}. In order to calculate this, the joint PPDF must be marginalized and then transformed to the variables of interest, and then marginalized again. Marginalization (Sivia, 1996) dispenses with nuisance variables by integrating over the range of all possibilities for that variable. Downton and Gray (2006) describe the details of these calculations. The resulting PDF is non-Gaussian but for simplicity of parameterization and understanding we approximate it as Gaussian. This approximation becomes more accurate as the anisotropic gradient, B_{ani}, increases. Making this approximation allows the uncertainty to be parameterized in terms of the standard deviations dB_{ani} and $d\Phi_{iso}$.

Downton and Gray (2006) show through a series of numerical modeling studies that accurate estimates of dB_{ani} and $d\,\Phi_{iso}$ can be obtained provided that $B_{ani} > dB_{ani}$. In practise this approximation is sufficient, since only anomalies whose fractional uncertainty are less than one should be considered. Note, for a constant noise level, as B_{ani} gets larger the fractional uncertainty decreases. Thus large anomalies have smaller fractional error than small anomalies.

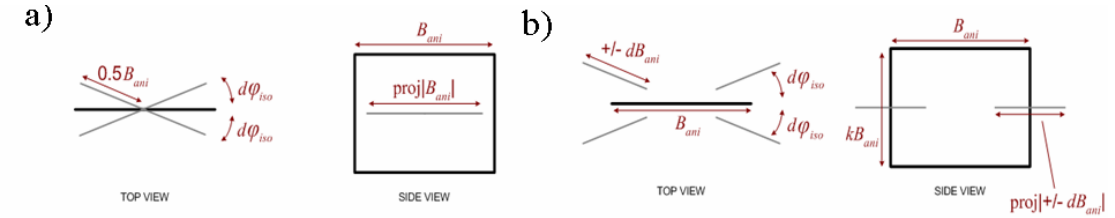

Figure 1. (a) Glyph shown in plan and profile view with azimuth uncertainty error bars. (b) Glyph shown in plan and profile view with azimuth and B_{ani} uncertainty error bars.

Visualization

In order to predict fracture intensity and orientation seismically, the interpreter is primarily interested in the B_{ani} and Φ_{iso} volumes and their related uncertainties. As typically she is interested in spatial changes for some geologic surface, the volume can be restricted to some time or horizon slice, reducing the dimensionality of the visualization problem. In order to visualize these four attributes simultaneously for an arbitrary surface from various viewing angles we developed a new graphical encoding (glyph). Other glyphs for depicting uncertainty in vector fields have been proposed by Wittenbrink et al., (1996). Our glyphs may be thought as a generalization of bidirectional vectors to planes (Figure 1a) allowing the interpreter to view the magnitude and orientation of the vector from some arbitrary viewing angle. The length and height of the glyph encode the magnitude of B_{ani} while the orientation of the glyph in plan view corresponds to the estimated isotropy axis. The uncertainty corresponding to Φ_{iso} may be communicated by displaying two bidirectional vectors, in a lighter colour, at plus and minus one standard deviation (Figure 1a). Further, the uncertainty of B_{ani} may be communicated by modifying these bidirectional vectors so that they are only displayed from $|B_{ani} - dB_{ani}|$ to $|B_{ani} + dB_{ani}|$ (Figure 1b).

Results

AVAZ inversion and uncertainty analysis were run on a small 3D seismic data set from Alberta, Canada centred over a known pinnacle reef. Figure 2 shows the B_{ani} and Φ_{iso} attributes and their related uncertainties for a time slice at 978 ms for a subset of the volume (context of the data shown in top right corner inserts). Figure 2a shows the data in plan view while Figure 2b shows that data oriented from the side looking slightly downward. In addition to the glyphs described in the previous section the B_{ani} attribute is displayed in colour. Note that at the edge of the survey the uncertainty in B_{ani} is larger than B_{ani}, as shown by the white uncertainty bars being larger than the black glyphs. To the left of Figure 2, over the pinnacle reef, the uncertainty is quite small adding credibility to the anomaly.

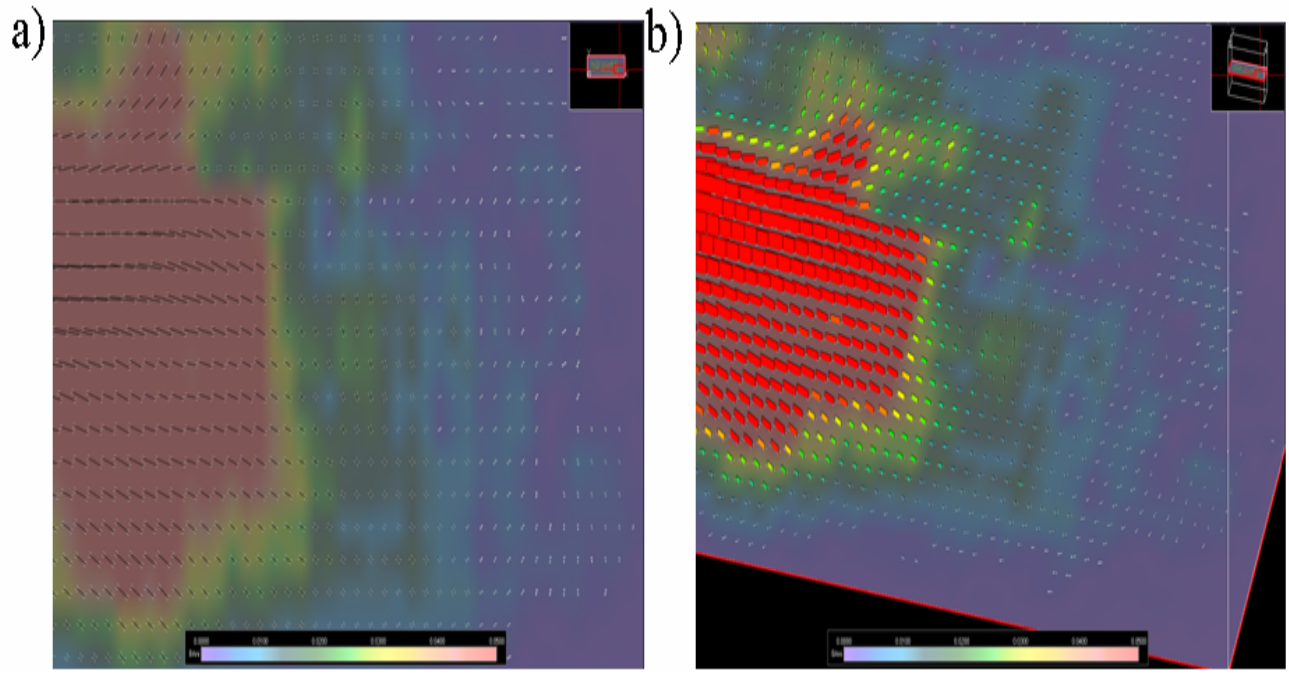

Figure 2. (a) The anisotropy gradient and symmetry axis shown in plan view (a) and an oblique view (b) over a pinnacle reef from Alberta, Canada.

Conclusions

We have shown a technique to estimate and visualize uncertainty due to random noise for both B_{ani} and Φ_{iso} that can be efficiently calculated as a by-product of the AVAZ inversion. The size of the uncertainty is proportional to the S/N ratio, is dependent on the geology and is influenced by the acquisition geometry. The estimate of B_{ani} will always be positive due to the nonlinearity of the inversion problem and thus it is important to ensure that a potential anomaly is much larger than its uncertainty. This will tend to favour large B_{ani} anomalies since their fractional uncertainty will be smaller than that of small anomalies for a given noise level. This type of analysis also identifies anomalies generated due to inadequate data acquisition geometries such as could happen where two 3D surveys are merged. Having performed this analysis it is important to point out that this uncertainty analysis is incomplete since factors such as systematic error are not accounted for.

Acknowledgments

Grateful thanks are due to Jan Dewar for her many useful suggestions in editing this paper.

References

Al-Marzoug, A.M., Neves, F.A., Kim, J.J. and Nebrija, E.L., 2004, P-wave anisotropy from Azimuthal velocity and AVO using wide-azimuth 3D seismic data. *SEG Expanded Abstracts*, 131-134.

Downton, J. and Gray, D., 2006, AVAZ parameter uncertainty estimation**.** *SEG Expanded Abstracts*, 234-237.

Downton, J. and Lines, L., 2001, AVO feasibility and reliability analysis. *CSEG Recorder*, **26**, no 6, 66-73.

Gray, D. and Todorovic-Marinic, D., 2004, Fracture Detection using 3D Azimuthal AVO. *CSEG Recorder*, **29,** no. 10, 5-8.

Ruger, A., 2002, Reflection coefficients and azimuthal AVO Analysis in anisotropic media. *SEG geophysical monograph series number* 10: Soc. Expl. Geophys.

Sivia, D.S., 1996, Data Analysis, a Bayesian tutorial, *Oxford University Press*.

Xu Y. and Li, Y., 2001, Uncertainties in azimuthal AVO analysis, *CSEG Expanded Abstracts*, 24 – 27.

Wittenbrink, C.M., Pang, A.T. and Lodha, S.K., 1996, Glyphs for visualizing uncertainty in vector fields. *IEEE Transactions on Visualization and Computer Graphics* 2, 3, 266–279.